

## Danielle Howe

Joint Department of Biomedical Engineering,  
North Carolina State University  
& University of North Carolina at Chapel Hill,  
Raleigh, NC 27695;  
Comparative Medicine Institute,  
North Carolina State University,  
Raleigh, NC 27695

## Nikhil N. Dixit

Department of Mechanical and  
Aerospace Engineering,  
North Carolina State University,  
Raleigh, NC 27695

## Katherine R. Saul<sup>1</sup>

Department of Mechanical and  
Aerospace Engineering,  
North Carolina State University, 3162  
Engineering Building III,  
1840 Entrepreneur Dr,  
CB 7910, Raleigh, NC 27695  
e-mail: ksaul@ncsu.edu

## Matthew B. Fisher<sup>1</sup>

Joint Department of Biomedical Engineering,  
North Carolina State University &  
University of North Carolina at Chapel Hill,  
4130 Engineering Building III,  
1840 Entrepreneur Drive, CB 7115,  
Raleigh, NC 27695;  
Comparative Medicine Institute,  
North Carolina State University,  
Raleigh, NC 27695;  
Department of Orthopaedics,  
University of North Carolina at Chapel Hill,  
NC 27599  
e-mail: mbfisher@ncsu.edu

# A Direct Comparison of Node and Element-Based Finite Element Modeling Approaches to Study Tissue Growth

*Finite element analysis is a useful tool to model growth of biological tissues and predict how growth can be impacted by stimuli. Previous work has simulated growth using node-based or element-based approaches, and this implementation choice may influence predicted growth, irrespective of the applied growth model. This study directly compared node-based and element-based approaches to understand the isolated impact of implementation method on growth predictions by simulating growth of a bone rudiment geometry, and determined what conditions produce similar results between the approaches. We used a previously reported node-based approach implemented via thermal expansion and an element-based approach implemented via osmotic swelling, and we derived a mathematical relationship to relate the growth resulting from these approaches. We found that material properties (modulus) affected growth in the element-based approach, with growth completely restricted for high modulus values relative to the growth stimulus, and no restriction for low modulus values. The node-based approach was unaffected by modulus. Node- and element-based approaches matched marginally better when the conversion coefficient to relate the approaches was optimized based on the results of initial simulations, rather than using the theoretically predicted conversion coefficient (median difference in node position 0.042 cm versus 0.052 cm, respectively). In summary, we illustrate here the importance of the choice of implementation approach for modeling growth, provide a framework for converting models between implementation approaches, and highlight important considerations for comparing results in prior work and developing new models of tissue growth. [DOI: 10.1115/1.4051661]*

## Introduction

Growth and remodeling of tissues are critical biological processes that can be influenced by biological stimuli such as cell type and density, hormones and other growth factors, and mechanical stimuli [1–7]. These processes may also be affected by changes in external stimuli that can result from conditions such as injury, disease, or therapeutic treatments. Modeling of these complex processes can lead to a deeper understanding of biological mechanisms while also providing predictive tools to study the impact of external stimuli.

The role of mechanics on biological growth and remodeling has been commonly studied via modeling (see a recent summary by Ambrosi et al. [7]). The majority of this work has used analytical models based on the theoretical framework of finite elasticity, finite growth, and constrained mixtures, which models growth through deformations [8], stress-dependent growth [9,10], and in the context of various tissue constituents [11], respectively. These models have been adapted and enhanced to model various tissues such as cartilage [12], tissues with unidirectional fibers [13], and charged fluids in a solid matrix [14]. However, analytical models alone cannot provide information within the context of complex, anatomically realistic three-dimensional (3D) tissue shapes.

Finite element (FE) models offer a way to simulate 3D tissue growth and study how growth is affected by biological and biomechanical conditions. FE modeling has been used to simulate growth in the context of biological tissues for many applications including joint morphogenesis and bone growth [15–21], skeletal muscle sarcomere shortening [22], cortical folding in the brain [23], tumor growth [24], abdominal aortic aneurysms [25–29], and cardiac growth and remodeling [30]. Many of these studies have implemented complex constitutive models of growth into FE analysis software packages through user material subroutine or custom plug-ins [22–30] to model specific biological mechanisms such as solid material deposition and remodeling, fluid influx, and cell division. Other studies have used existing capabilities within FE software packages to induce growth using simple surrogate mechanisms such as thermal expansion [15,17,19,20,31] and osmotic swelling [32,33] to simulate biological processes involved in growth. These approaches have proven capable of capturing realistic morphologies given physiological stimuli in specific cases such as diarthrodial joint development [15,16]. In these approaches, growth stimuli are applied as a temperature differential to induce thermal expansion or an intracellular to extracellular solute concentration differential to induce swelling.

Whether complex or simple, approaches used to simulate growth are at their essence applied in either a node-based [15–17,19,31] or element-based [20,32] fashion. Node-based approaches achieve growth by dictating linear (one-dimensional) expansion of the distance between sets of nodes while element-

<sup>1</sup>Corresponding authors.

Manuscript received August 15, 2020; final manuscript received June 25, 2021; published online September 1, 2021. Assoc. Editor: Katherine Yanhang Zhang.

based approaches achieve growth by dictating volumetric (3D) expansion of the volume of each element. This choice of approach may in and of itself influence the growth predicted using these methods, irrespective of the specific growth relationship being applied. In addition, because different growth modeling approaches are used across studies, it is unclear how to directly relate growth models that use node- and element-based approaches, or how one might implement the same growth law in different FE modeling platforms that use these two different mechanisms. When using FE models to predict tissue growth and development, it is important to consider how the choice of expansion implementation impacts resulting changes in morphology. Grytsan et al. began to explore this area by comparing isotropic, in-plane, or in-thickness growth kinematic approaches in the context of abdominal aortic aneurysm growth [26]. Similarly, comparison of the influence of element- and node-based approaches is needed since two commonly used FE software packages with existing expansion capabilities use different mechanisms. Specifically, several studies have utilized thermal expansion capabilities available in ABAQUS [15,17,19,31], which utilizes a node-based approach, and cell growth capabilities available in FEBIO [32,33], which uses an element-based approach, to simulate growth of biological tissues.

One possible method to fluently apply growth models in both node- and element-based approaches is to determine an idealized mathematical relationship between the approaches. Within the context of thermal expansion, one-dimensional and 3D expansions are related such that the volumetric thermal expansion coefficient ( $\alpha_V$ ) equals 3x the linear thermal expansion coefficient ( $\alpha_L$ ) for small changes in temperature and infinitesimal deformations within an isotropic material [34]. However, the assumption of infinitesimal deformations is inconsistent with many examples of biological growth. Therefore, the goal of this work was to (1) explore the isolated influence of node- or element-based approaches of growth and (2) mathematically and computationally explore the relationship and scaling of coefficients between an element-based (volumetric) model using osmotic swelling and a node-based (linear) model using thermal expansion. We explored several important variables of implementation including a conversion coefficient to relate the node- versus element-based approaches, number of iterations, and material modulus. Since the element-based approach in FEBIO implements growth within a constitutive relationship relating stress and strain while the node-based approach does not, we hypothesized that the element-based approach would tend to predict less growth than node-based approach when using an idealized conversion coefficient, and tissue material properties would affect comparisons across approaches, with stiffer materials restricting growth in the element but not node-based approach.

## Methods

**Model Framework.** To test the isolated impact of choice of node- or element-based approaches, we used existing expansion capabilities within two FE solvers—FEBIO and ABAQUS CAE—which can be used as surrogates to produce a desired expansion of a tissue as a result of growth. The element-based modeling approach of tissue growth was developed in FEBIO (version 2.6.4, FEBio Software Suite, Salt Lake City, UT) [35] and postprocessed in POST-VIEW (version 2.0.0, FEBio Software Suite, Salt Lake City, UT). All FEBIO simulations were controlled through MATLAB (version 9.5, Mathworks, Portola Valley, CA) using code adapted from the geometry and image-based bio-engineering add-on [36], an open-source MATLAB toolbox that allows users to run simulations in FEBIO through a MATLAB script. In FEBIO, osmotic swelling was used to simulate volumetric tissue growth [32,37]. Growth was implemented through Eq. (1), in which an increased ratio of internal ( $C_r$ ) to external solute concentration ( $C_e$ ) with constant solid volume fraction ( $\phi$ ) causes an expansion ( $\Delta V$ ) of elemental volume ( $V$ )

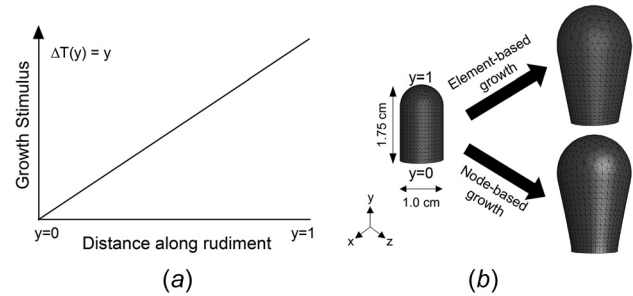


**Fig. 1 (a) Growth stimulus ( $\Delta T(y)$ ) was implemented as a linear function of normalized distance along the rudiment and (b) growth of a simple rudiment geometry was simulated for 10 cycles of growth for element-based and node-based approaches**

$$\Delta V = V * (C_r / C_e + \phi - 1) \quad (1)$$

The node-based modeling approach of growth was developed in ABAQUS CAE (version 6.13, Dassault Systems, Vélizy-Villacoublay, France) and controlled through a Python script. Models were based on existing literature using thermal expansion [15,16], implemented through Eq. (2), in which increased temperature ( $\Delta T$ ) with linear thermal expansion coefficient ( $\alpha_L$ ) causes expansion ( $\Delta L$ ) of the distance ( $L$ ) between nodes

$$\Delta L = L * \alpha_L * \Delta T \quad (2)$$

To relate the expansion produced by osmotic swelling to that produced by thermal expansion, Eq. (1) was equated to the volumetric thermal expansion equation shown in Eq. (3), using a volumetric thermal expansion coefficient ( $\alpha_V$ )

$$\Delta V = V * \alpha_V * \Delta T \quad (3)$$

The system was solved for  $C_r$  to produce the following relationship:

$$C_r = C_e (\alpha_V * \Delta T - \phi + 1) \quad (4)$$

Equation (4) was substituted into Eq. (1) and implemented in the element-based approach.

**Model Implementation.** For all simulations, the initial geometry was implemented as a rudiment, which has been used as a basis to simulate diarthrodial joint morphogenesis [15,16]. The geometry was created in ABAQUS and composed of a cylinder (1 cm diameter, 1.25 cm height) with a hemispherical end (1 cm diameter) (Fig. 1). A tetrahedral (tet4) mesh was applied, composed of 13,744 elements with an average volume of 0.0899 mm<sup>3</sup>, each connected by four nodes, and a total of 2822 nodes. The geometry and mesh were imported into PRE-VIEW (version 1.20.4, FEBio Software Suite, Salt Lake City, UT), the FEBIO preprocessing software, to create the FEBIO geometry file, such that both approaches had identical initial geometry and mesh. Preliminary studies were performed to evaluate how the number of elements impacts simulation time. Simulations were performed using the rudiment geometry with a mesh composed of elements with approximately double (28,202 elements, average volume of 0.0439 mm<sup>3</sup>) and triple (44,358 elements, average volume of 0.0280 mm<sup>3</sup>) the number of elements in the initial mesh. Initial rudiment simulations ranged from ~10 min of computational time for both the element- and node-based approaches. For the element-based approach, computational time increased by ~5 times for double the number of elements and ~8 times for triple the number of elements. For the node-based approach, computational time increased by ~1.4 times for double the number of elements and ~2 times for triple the number of elements.

Growth stimulus was applied as a linear function of normalized distance along the rudiment height such that the growth stimulus was zero at the base of the rudiment and one at the top of the rudiment (Fig. 1). This stimulus was implemented through Eqs. (2) and (4) as a temperature differential ( $\Delta T$ ). When simulating tissue growth, this equation has been implemented in previous models to simulate a biological growth stimulus, specifically as a function of chondrocyte density when simulating long bone morphogenesis [15,16,38], and was chosen here as a simple model to highlight the isolated effects of node- versus element-based approaches, rather than to capture complex growth stimuli.

Boundary conditions for all simulations were applied by fixing all nodes on the bottom surface of the rudiment in the  $y$ -direction (longitudinal direction) and fixing the topmost central node to maintain  $x$ - and  $z$ -coordinates (transverse directions) equal to zero. For all ABAQUS simulations, isotropic, homogeneous, neo-Hookean material properties were applied. Thermal expansion properties, defined by  $\alpha_L$  in Eq. (2), were applied to the whole model, with temperature applied to each node as a function of its  $y$ -position. For all FEBIO simulations, isotropic material properties were assigned to the rudiment as a solid mixture of a neo-Hookean material, defined by elastic modulus and Poisson's ratio, and a cell growth material, defined by  $C_r$  and  $C_e$ , and  $\varphi$  via Eq. (1).  $C_r$  was defined by the relationship in Eq. (4). The  $C_e$  and  $\varphi$  terms cancel out when substituting Eq. (4) into Eq. (1), so these values should not affect comparisons between approaches. To verify that  $\varphi$  did not impact results, simulations of the element-based approach were performed for values of  $\varphi$  ranging from 0.000001 to 0.9 (possible values are 0–1) with  $C_e=2000$ ,  $\alpha_V=0.27$ , and a modulus of 1 kPa (Table S1 available in the Supplemental Materials on the ASME Digital Collection). Similarly, simulations of the element-based approach were performed for values of  $C_e$  ranging from 2 to 20,000 with  $\varphi=0.000001$ ,  $\alpha_V=0.27$ , and a modulus of 1 Pa for  $C_e=2$ , 20, and 200 and 1 kPa for  $C_e=2000$  and 20,000 (Table S2 available in the Supplemental Materials on the ASME Digital Collection). For an appropriate modulus value for the neo-Hookean material, simulation results were minimally affected by  $\varphi$  and  $C_e$ . For the simulations presented in this paper,  $C_e$  and  $\varphi$  were set to 2000 and 0.000001, respectively. Material properties were applied to each individual element using a MATLAB script modified from the geometry and image-based bio-engineering add-on open source spatially varying material parameters demonstration file (DEMO\_spatially\_varying\_material\_parameters). For this study, the neo-Hookean material properties were held constant within a given simulation while the cell growth material properties varied by element.

For all node-based simulations,  $\alpha_L$  was arbitrarily set equal to 0.08. For all element-based simulations,  $\alpha_V$  was defined relative to  $\alpha_L$  using conversion coefficient ( $C$ ), in the following relationship:

$$\alpha_V = C * \alpha_L \quad (5)$$

To determine the appropriate conversion coefficient, element-based simulations were performed using  $C = 1, 2, 3, 4$ , and 5. All simulations varying the conversion coefficient used neo-Hookean material properties, with elastic modulus of 1 kPa and Poisson's ratio of 0.49. To evaluate the effect of material properties, additional simulations were performed with elastic moduli of 1 kPa, 10 kPa, 100 kPa, 500 kPa, 1 MPa, 5 MPa, 10 MPa, 100 MPa, and 1 GPa and a constant Poisson's ratio of 0.49, for both element and node-based approaches with  $C = 3$ .

All simulations were iterated through 10 growth cycles. After each cycle, growth was applied to the new geometry as a function of normalized distance along the rudiment. No remeshing was done between cycles since small relative changes in element size would not impact growth (i.e., the sum of the growth of two elements will produce the same growth as one element that is twice the size, by Eq. (3)). Maximum height and width of the rudiment were recorded after each cycle, and percent differences were calculated between modeling approaches.

Next, element-based simulations were performed using theoretically determined conversion coefficients. As described earlier, the theoretical conversion coefficient relating volumetric and linear expansion should be  $C = 3$ , assuming infinitesimal changes in temperature [34]. Therefore,  $C = 3$  was termed the *ideal* theoretical conversion coefficient. However, without assuming infinitesimal changes in temperature, an *expanded* theoretical conversion coefficient relationship was derived using the parameters in this study, in which  $\Delta T$  ranges from 0 to 1 (derivation shown in Supplemental Material)

$$C = 3 + 0.24\Delta T + 0.0064\Delta T^2 \quad (6)$$

An element-based simulation was performed with the expanded conversion coefficient defined by Eq. (6), applied on an element-by-element basis. The modulus was defined as the value that produced most similar results between the element- and node-based simulations from the sensitivity experiment varying modulus values above.

Next, an optimized element-based simulation was performed using a constant *optimized* conversion coefficient determined based on results from sensitivity simulations varying values of  $C$  above. Linear interpolation was used to identify the intersection of the element-based and node-based predictions for both height and width (Figs. 3(b) and 3(c)), where the rudiment dimensions would be assumed to be equal for node- and element-based approaches. The optimized conversion coefficient was defined as the mean of the intersection values computed for height and width. The same modulus used for the theoretical simulation was implemented for this optimized simulation. The process of performing conversion coefficient sensitivity simulations, interpolating an optimized conversion coefficient, followed by an optimized simulation took approximately 1 h.

Further analysis was done to compare results from element-based simulations using the ideal theoretical, expanded theoretical, and optimized conversion coefficients to results from the node-based simulation on a node-by-node basis. Distances between corresponding nodes in simulations performed with both approaches were calculated as the root-mean-square error in position of each node for the element-based approach relative to the corresponding node in the node-based approach, using a custom MATLAB code. The median and interquartile ratio (IQR) of these nodal differences were calculated for each element-based approach relative to the node-based approach. Differences were also calculated as a normalized value, relative to total displacement of each node in the node-based approach. Both raw and normalized differences were statistically compared using Friedman tests with Dunn's posthoc analysis (overall alpha set at 0.05). Findings were confirmed using two alternative geometries: a cylinder (1.25 cm height, 0.5 cm radius) with a hemispherical concave surface (0.4 cm radius) and a cylinder (1.25 cm height, 0.5 cm radius) with a shallow convex surface that increased the height by 0.1 cm (Fig. S3 available in the Supplemental Materials on the ASME Digital Collection).

## Results

Rudiments grew in a qualitatively similar manner for the two approaches throughout the 10 growth cycles (Fig. 2). The rudiments generally showed the most outward growth toward the top of the rudiment while remaining approximately the same size at the base (Fig. 3(a)). Quantitatively, higher conversion coefficients resulted in greater overall growth in the element-based simulations, and the simulation using a conversion coefficient of 3 resulted in predicted rudiment size most similar to the node-based simulation. Specifically, element-based simulations were 25%, 14%, 4%, 8%, and 20% different in height compared to the node-based simulation for conversion coefficients  $C = 1, 2, 3, 4$ , and 5, respectively (Fig. 3(b)). Rudiment widths were also most similar between the two approaches for element-based simulations using

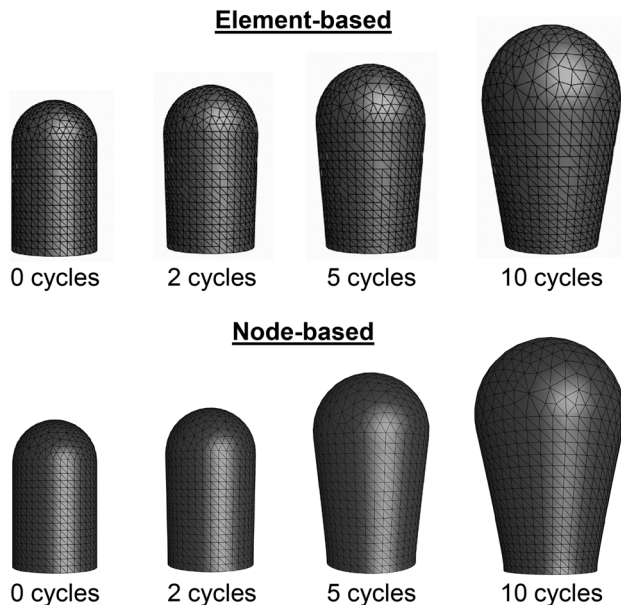


**Fig. 2** Rudiment geometries grew similarly in element- and node-based simulations with  $E = 1$  kPa and a conversion coefficient  $C = 3$ . Geometries shown after 0, 2, 5, and 10 cycles of growth.

a conversion coefficient of  $C = 3$  (Fig. 3(c)). However, widths were nearly as similar between the approaches when the conversion coefficient of  $C = 4$  was used. Specifically, element-based simulations were 32%, 20%, 7%, 8%, and 23% different in width compared to the node-based simulation for conversion coefficients  $C = 1, 2, 3, 4,$  and  $5$ , respectively.

The impact of modulus ranging from 1 kPa to 1 GPa was next evaluated. A conversion coefficient  $C = 3$  was used for the element-based simulation since this produced the closest results to the node-based simulation in the prior simulation set. Element-

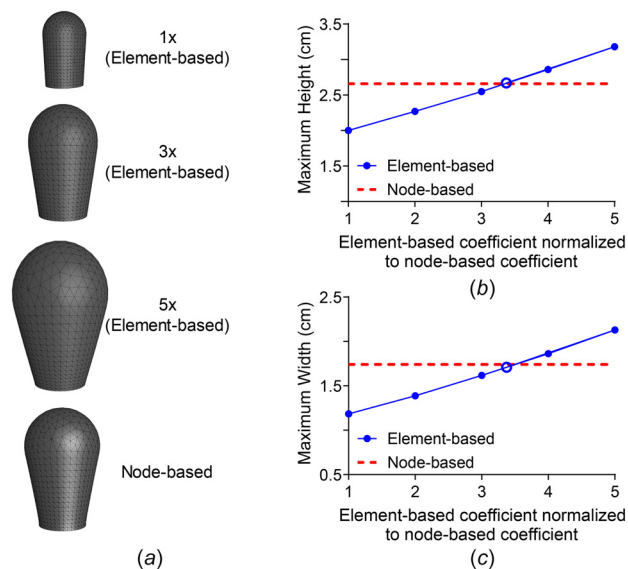


**Fig. 3** The element-based approach produced a geometry most similar to the node-based approach for a conversion coefficient  $C = 3$ . (a) Rudiment geometries after 10 cycles of growth for element-based simulations with conversion coefficients  $C = 1, 3,$  and  $5$ . Maximum rudiment height (b) and width (c) after 10 cycles of growth with the conversion coefficient  $C = 1-5$ . Results from simulations with interpolated optimized conversion coefficient ( $C = 3.375$ ) are represented by the open circle.

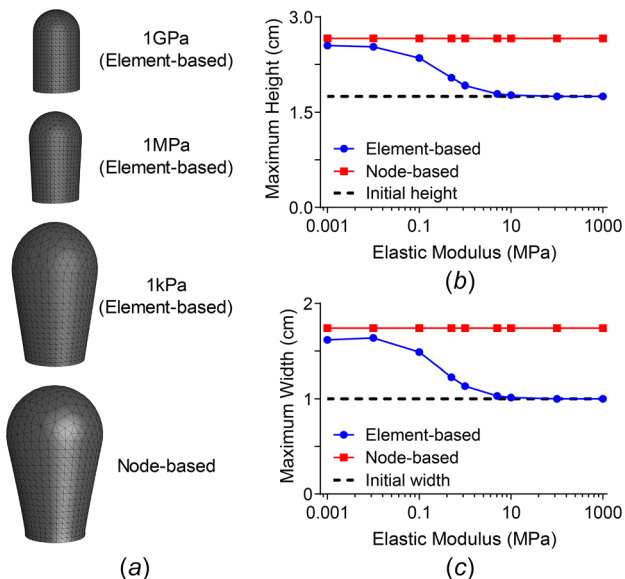


**Fig. 4** Modulus influenced growth in element but not node-based simulations. (a) Rudiment geometries after 10 cycles of growth for moduli of 1 GPa, 1 MPa, and 1 kPa. Maximum rudiment height (b) and width (c) after 10 cycles of growth modulus values varying from 1 Pa–1 GPa. Element-based simulations were performed with a conversion coefficient  $C = 3$ .

based geometries were most similar to node-based geometries for simulations with low modulus values (Fig. 4(a)). Over the tested modulus range of 1 kPa to 1 GPa, element-based growth decreased in a sigmoidal manner as modulus increased, with growth decreasing most from 0.1 MPa to 10 MPa (Figs. 4(b) and 4(c)). The element-based simulations at 1 GPa and 100 MPa showed no growth from the initial geometry. In contrast, node-based growth was unaffected by modulus, as expected.

Next, the effect of number of growth iterations was studied. Over the 10 cycles, the node-based simulation grew steadily with increased cycle number (Fig. 5(a)). At the lowest modulus ( $E = 1$  kPa), the element-based simulation behaved similarly. As modulus increased, the amount of growth in the element-based simulations decreased uniformly between consecutive cycles, with the simulation using a high modulus ( $E = 1$  GPa) having no growth between any cycles. Additionally, both absolute and percent differences between the modeling approaches increased with the number of cycles (Fig. 5(b)). Overall, node and element-based approaches were most similar at a low modulus ( $E = 1$  kPa), with 4% difference in height and 7% in width after 10 cycles (Fig. 5(b)). Model predictions differed the most for  $E = 1$  GPa, with 34% difference in height and 42% in width after 10 cycles.

Once the effects of conversion coefficient, modulus, and cycles were assessed, the ideal theoretical, expanded theoretical, and optimized conversion coefficients were compared in their ability to produce an element-based simulation that matched the node-based simulation. A modulus of 1 kPa produced the most similar results between modeling approaches (Fig. 4) and was used for the following simulations. From earlier sensitivity analyses, a conversion coefficient  $C = 3$  produced more similar results between element and node-based approaches than other conversion coefficients, validating it as the ideal theoretical conversion coefficient (Fig. 3). By plotting the nodes from the resulting geometries, it was clear that the element-based simulation using the ideal theoretical conversion coefficient resulted in a rudiment that was smaller than the node-based simulation (by 4% and 7% in height and width, respectively) (Fig. 6(a)). Using the expanded theoretical conversion coefficient (ranging from 3 to 3.246 by Eq. (6)) brought the element-based approach closer to the geometry from the node-based approach, within 2% and 4% of the final node-

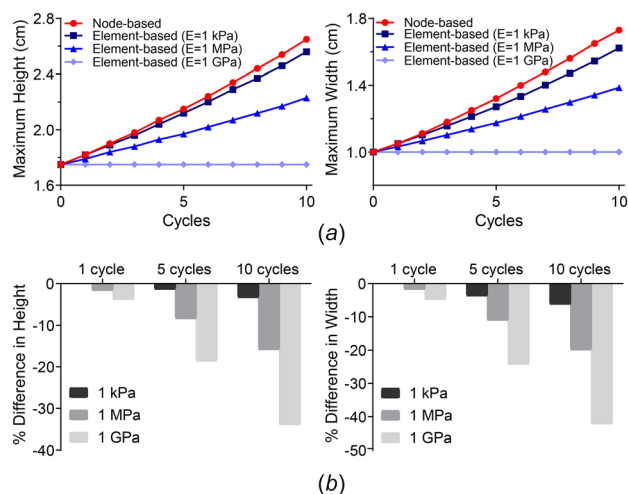


**Fig. 5 Differences between element and node-based approaches increased with increasing cycles. (a) Maximum height and width of the rudiment over 10 cycles for the node-based and element-based approaches for moduli ranging from 1 kPa to 1 GPa. Since the node-based approach was unaffected by modulus, values are only shown once. (b) Percent difference in maximum height and width of element-based simulations relative to the node-based simulation after 1, 5, and 10 cycles.**

based height and width, respectively (Fig. 6(a)). Finally, we used an optimized conversion coefficient interpolated based on height and width values, respectively (Figs. 3(b) and 3(c)). The average of these was  $C = 3.375$ . The geometry from the element-based simulation using this optimized conversion coefficient was more similar to that of the node-based approach than for previous simulations (Fig. 6(a)). Final height (2.67 cm) and width (1.71 cm) were, respectively, within 1% and 2% of node-based results.

Comparing the element-based simulations to the node-based simulation on a node-by-node basis revealed that the greatest differences in all cases occurred toward the center of the rudiment (Fig. 6(b)). The element-based simulation using the ideal theoretical conversion coefficient appeared to have the most striking differences, with large differences toward the upper portion of the rudiment. Use of the expanded theoretical conversion coefficient reduced these differences, and the optimized conversion coefficient brought the results closer still. The most marked improvement relative to other simulations was observed near the surface of the upper portion of the rudiment, where nodes matched very closely when using the optimized conversion coefficient (Fig. 6(b)). Quantitatively, the difference in nodal positions of the element-based simulations relative to the node-based simulation showed non-normal distributions. Differences were significantly smaller using the optimized conversion coefficient (median 0.042 cm, IQR 0.032–0.054 cm) than either the ideal theoretical or the expanded theoretical conversion coefficient ( $p < 0.05$ ). Additionally, differences were smaller using the expanded theoretical conversion coefficient (median 0.052 cm, IQR 0.038–0.067 cm), than the ideal theoretical conversion coefficient (median 0.055 cm, IQR 0.036–0.083 cm) ( $p < 0.05$ ). Although the median values were not far apart between simulations using the theoretical conversion coefficients, the distribution of values was much smaller using the expanded theoretical conversion coefficient.

When differences between nodal positions were normalized to the total nodal displacement in the node-based approach, the comparison of the final three element-based simulations appeared very similar. The nodes differed by a median of 0.33 (IQR 0.17–0.81), 0.34 (IQR 0.15–0.86), and 0.33 (IQR 0.09–0.93) times their total displacement for the element-based approach with the ideal theoretical, expanded theoretical, and optimized conversion coefficients, respectively (Fig. S2 available in the Supplemental Materials on the ASME Digital Collection). The greatest normalized

differences for all three models occurred toward the lower half of the rudiment where node displacements are small (Fig. S2(a) available in the Supplemental Materials).

When considering alternate geometries, similar growth between modeling approaches was achieved with the expanded theoretical conversion coefficient, but differences were slightly larger compared to simulations with the rudiment geometry (Fig. S3 available in the Supplemental Materials). For a cylinder with a hemispherical concave surface, the element-based simulation was 5% larger in height and 5% smaller in width than the node-based simulation, and node positions differed by a median of 0.035 cm (Fig. S3(a) available in the Supplemental Materials). Additionally, after growth, the concave surface appeared shallower for the node-based approach than the element-based approach. Using a cylinder with a convex surface, the element-based simulation was 8% and 13% smaller in height and width, respectively, than the node-based approach, and node positions differed by a median of 0.057 cm (Fig. S3(b) available in the Supplemental Materials). Optimized conversion coefficients were interpolated between  $C = 3$  and  $C = 4$  for the geometries with a concave ( $C = 3.1$ ) and convex ( $C = 4$ ) surface, in the same manner described for the rudiment geometry (Tables S3 and S4 available in the Supplemental Materials). Using the optimized conversion coefficients, the height and width of node and element-based simulations were, respectively, within 5% and 7% for the concave geometry (Table S3 available in the Supplemental Materials) and 1% and 0.1% for the convex geometry (Table S4 available in the Supplemental Materials). Additionally, final node positions between element and node-based approaches differed by a median of 0.038 cm for the concave surface geometry and 0.058 cm for the convex surface geometry.

## Discussion

In this study, we explored the isolated effects of the type of growth model implementation on simulated tissue growth using existing element- and node-based approaches within FE software packages. Our simulations reveal how choice of different implementation parameters—including modulus, number of iterations, conversion coefficient, and geometries—affect predictions and determined under what conditions node- and element-based approaches predict similar resulting geometries. This work is essential for understanding how growth models can be consistently implemented within individual FE platforms or allow for fair comparisons of simulations between FE platforms. We found that tissue modulus affected growth in the element-based, but not node-based, approach, such that the approaches matched most closely for low modulus values. This confirmed our hypothesis that higher modulus would restrict growth in the element-based, but not the node-based, approach. Further, we found that to create comparable geometries in response to the same growth stimulus, theoretical conversion coefficients for the element-based approach resulted in similar overall growth as the node-based approach, which could be further improved using an optimized conversion coefficient.

Several sensitivity analyses revealed the role of the conversion coefficient, tissue stiffness, and cycle number in creating differences between element- and node-based approaches. The first set of simulations showed that approaches matched most closely for a conversion coefficient of  $C = 3$ . This is consistent with thermal expansion theory, in which  $\alpha_V = 3\alpha_L$  for infinitesimal changes in temperature [34]. However, the simulations testing the effect of modulus suggest that care must be taken to use low modulus values relative to the expansion stimulus during growth simulations if comparisons are to be made to equivalent node-based approaches. On the other hand, inclusion of a realistic tissue stiffness in element-based approaches may be an important consideration for directly capturing principles of experimentally measured tissue growth. These results also suggest an alternate approach may be useful, in which sequential simulations may be needed for growth stimuli that depend on modulus, such as mechanical stimuli that depend on regional stresses or strains throughout the

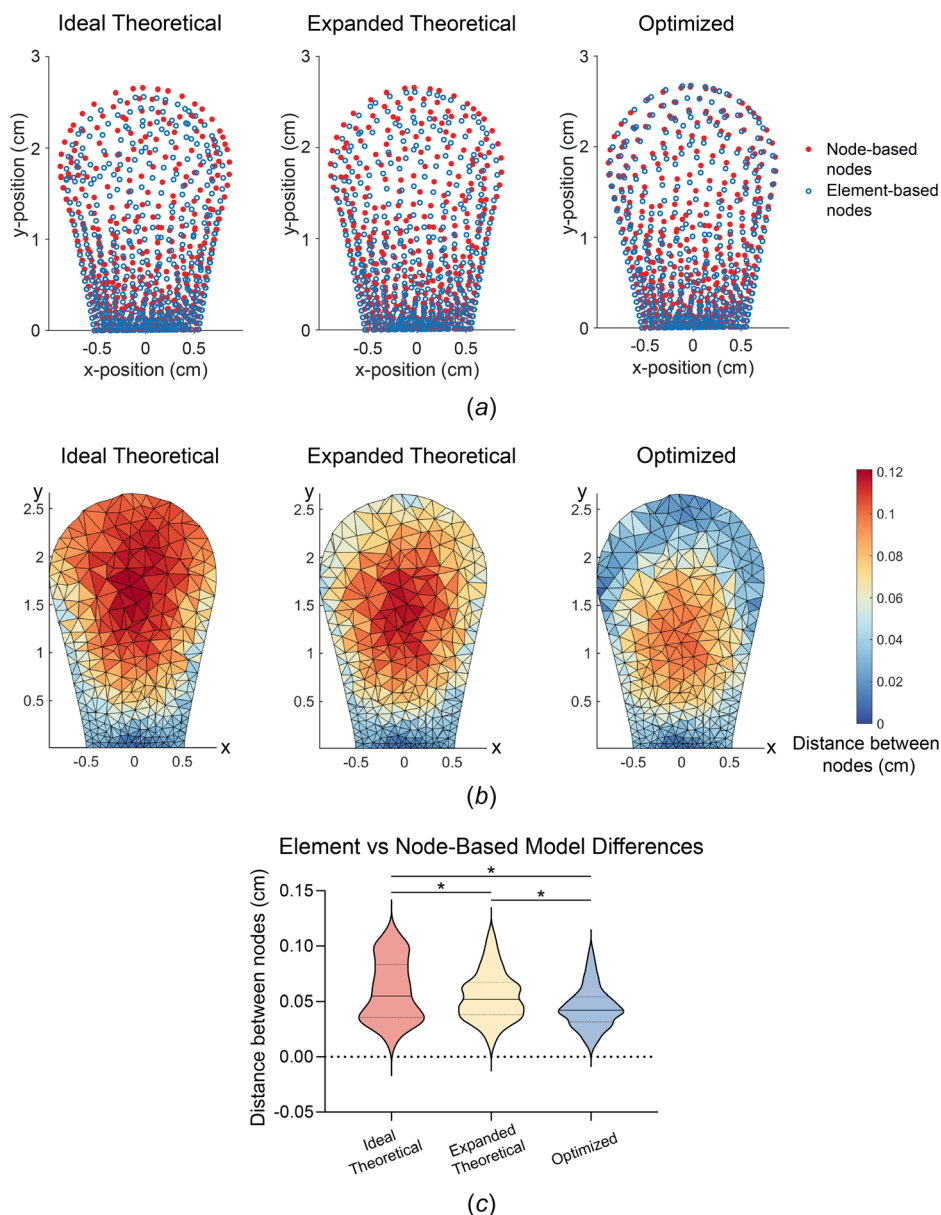


**Fig. 6** The positions of the nodes in the element and node-based simulations aligned more closely using the expanded theoretical conversion coefficient ( $3 + 0.24\Delta T + 0.0064\Delta T^2$ ) than using the ideal theoretical conversion coefficient ( $C = 3$ ), but results matched most closely using an optimized conversion coefficient ( $C = 3.375$ ). (a) Nodes from three element-based simulations overlaid on nodes from the node-based simulation, projected onto the  $x$ - $y$  plane. Nodes were down-sampled for visual clarity. (b, c) Distance (cm) between corresponding nodes of the element-based approach compared to the node-based approach shown as (b) heat maps on the node-based rudiment cross section and (c) violin plots of the data. \* indicates  $p < 0.05$  between groups.

volume of the tissue. In these cases, one simulation may be needed to determine the mechanical loading and growth stimuli, and a second simulation may be needed to apply the associated expansion [15–17]. In this way, separate simulations can allow for a realistic modulus (e.g., approximately 1.1 MPa for unmineralized cartilage [39]) to be applied during mechanical simulations, separate from the modulus used for growth simulations, where users may wish to implement a low modulus (such as 1 kPa or lower) to avoid restricting growth. Finally, our simulations illustrated that the number of growth cycles influenced outcome, with differences between approaches increasing with additional cycles. Because a growth stimulus depends on geometry and will differ as geometries diverge, small differences in initial cycles will increase with additional growth cycles. This would likely have

implications in modeling long-term growth in which substantial changes in size occur.

When examining the conversion coefficient needed to convert between node- and element-based approaches, the ideal theoretical conversion coefficient resulted in some differences in prediction between the two approaches. Including noninfinitesimal changes in temperature in the derivation of the expanded theoretical conversion coefficient improved consistency between the element- and node-based approaches and tightened the distribution of node-by-node differences. Specifically, since the value of the expanded theoretical conversion coefficient increased along the height of the rudiment, proportional to the growth stimulus, this coefficient decreased discrepancies toward the top of the rudiment that were observed using the ideal theoretical coefficient. Notably,

an optimized conversion coefficient derived from the sensitivity analyses was best able to generate matched prediction in the element-based approach compared to the node-based approach. The optimized coefficient ( $C = 3.375$ ) was slightly larger than the ideal or expanded theoretical prediction for the conversion between approaches ( $C = 3\text{--}3.246$ ). It would be possible to improve the agreement between approaches by implementing a coefficient as a quadratic function of temperature, like that in Eq. (6), in which the conversion coefficient is smaller at the base of the rudiment, where smaller changes in temperature were applied, than the top of the rudiment. The improvement when using the slightly larger optimized coefficient could be explained by the fact that elements are constrained by growth of adjacent elements that share nodes and faces in the element-based approach, unlike the node-based approach, where nodes move independently.

To highlight this point further, the use of the same initial geometry allowed us to compare the models on a node-by-node basis. Overall, using the ideal theoretical, expanded theoretical, and optimized conversion coefficients, the node-by-node differences between approaches were fairly small, with  $<0.10$  cm error for almost all nodes. However, more detailed regional comparisons of differences in node positions showed that the predicted shapes varied slightly. Greatest differences between the approaches were seen toward the center of the rudiment, which may stem from differences initiated at the base of the rudiment. Elements at the base of the rudiment experienced some growth stimulus in the element-based approach, since the  $y$ -coordinate of the centroid is greater than zero, causing slight expansion at the base of the rudiment. However, base nodes in the node-based approach experienced no growth since their  $y$ -coordinates are zero. Therefore, nodes toward the base of the rudiment in the element-based approach experienced greater growth than those in the node-based approach, causing differences in both radial and vertical expansion between these nodes, which may propagate upward to the central portion of the rudiment. This can also explain differences at the base of the rudiment, where the element-based approach was wider than the node-based approach. Once the differences between the element- and node-based approaches were normalized by node displacement, the median normalized differences showed little variation between the three conversion coefficients. Across all simulations, normalized distances between nodes were greatest toward the bottom of the rudiment, where total displacements were very small. Thus, although some normalized distances were large, this is not a concern due to the very small total displacement in this area.

There are some limitations that should be considered regarding the current study. This study implements tissue growth in simplified simulations, with a basic geometry, linear growth stimulus, and homogeneous, linear-elastic, isotropic, material properties, which are not intended to be representative of growth that occurs in vivo. It is important to note that this study is not intended to validate or compare specific models of growth stimuli, but rather to highlight how parameter or platform selection can influence simulation prediction in perhaps unintentional ways and can be carefully chosen to avoid these discrepancies. Because the goal of this study was to evaluate the isolated influence of modeling approach on predictions made with a growth model given the same growth stimulus, we purposely chose a simple stimulus to best elucidate the effects of parameter selection during implementation. However, it is possible that the influence of modeling approach may be dependent to a certain extent on the specific growth stimuli being implemented; this should be considered in future work. Additional simulations with multiple input geometries showed that the results shown here for the rudiment geometry behaved similarly in other geometries, and similar growth between element- and node-based approaches could be achieved using the expanded theoretical conversion coefficient. However, the small differences indicate that more complex geometries could expand differences in simulation predictions when comparing element- and node-based approaches, particularly for geometries

with sharp edges. Similarly to the rudiment, using a calculated optimized conversion coefficient for the concave and convex geometries improved agreement between modeling approaches. Although the optimized conversion coefficients varied slightly between geometries ( $C = 3.1, 4.0, \text{ and } 3.375$  for the concave, convex, and rudiment geometries, respectively), these optimized simulations resulted in similar median differences in node positions (0.035 cm, 0.057 cm, and 0.042 cm, respectively). These results indicate that best comparison between modeling approaches can be obtained if an optimized conversion coefficient is calculated for each new geometry. Similar adjustments may be necessary for implementation of more complex growth laws or growth stimuli. Additionally, this study did not evaluate which growth mechanism produces results more similar to growth observed in vivo. These types of comparisons, such as those done in the context of abdominal aortic aneurysms [26], are useful but may be tissue-specific and would be interesting to investigate in future studies. Thus, although the current study begins to compare mechanisms, specifically node- versus element-based growth, more work can be done to improve understanding how different growth modeling approaches and methodologies impact the predicted morphology of simulations.

In conclusion, this study developed a framework for comparing element-based and node-based FE models of tissue growth to allow the same growth law to be applied across platforms with different growth mechanisms. Overall, we found that two different approaches for modeling growth resulted in comparable geometries when appropriate parameters were selected; however, small differences in the morphologies were present. When using FE modeling to study growth, it should be considered that the chosen growth law and modeling approach may impact the predicted morphology. For example, node-based approaches may be able to produce finer features, while element-based approaches may more realistically capture how tissue material properties can constrain or influence growth. The relationships outlined in this work can be applied as a starting point to translate models between node- and element-based growth approaches. By allowing for comparisons across studies and translation of models, this work can increase model reproducibility and accelerate research and modeling of tissue growth.

## Acknowledgment

The programs written in Python and MATLAB used to perform simulations in this study are freely available on GitHub.<sup>2</sup> Research in this publication was supported by the National Center for Simulation in Rehabilitation Research (NIH P2CHD065690) and the National Institute of Arthritis and Musculoskeletal and Skin Diseases of the U.S. National Institutes of Health (R01AR071985). The content is solely the responsibility of the authors and does not necessarily represent the official views of the National Institutes of Health.

## Funding Data

- National Center for Simulation in Rehabilitation Research (Grant No. NIH P2CHD065690; Funder ID: 10.13039/100000071).
- National Institute of Arthritis and Musculoskeletal and Skin Diseases of the U.S. National Institutes of Health (Grant No. R01AR071985; Funder ID: 10.13039/100000069).

## References

- [1] Wang, J. H., and Thampatty, B. P., 2006, "An Introductory Review of Cell Mechanobiology," *Biomech. Model. Mechanobiol.*, **5**(1), pp. 1–16.
- [2] Decker, R. S., Koyama, E., and Pacifici, M., 2014, "Genesis and Morphogenesis of Limb Synovial Joints and Articular Cartilage," *Matrix Biol.*, **39**, pp. 5–10.

<sup>2</sup><https://github.com/Translational-Orthopaedic-Research-Lab/Node-and-Element-Based-FE-Growth-Models>

- [3] Arvind, V., and Huang, A. H., 2017, "Mechanobiology of Limb Musculoskeletal Development," *Ann. N. Y. Acad. Sci.*, **1409**(1), pp. 18–32.
- [4] Galloway, M. T., Lalley, A. L., and Shearn, J. T., 2013, "The Role of Mechanical Loading in Tendon Development, Maintenance, Injury, and Repair," *J. Bone Jt. Surg. Am.*, **95**(17), pp. 1620–1628.
- [5] Discher, D. E., Mooney, D. J., and Zandstra, P. W., 2009, "Growth Factors, Matrices, and Forces Combine and Control Stem Cells," *Science*, **324**(5935), pp. 1673–1677.
- [6] Humphrey, J. D., Dufresne, E. R., and Schwartz, M. A., 2014, "Mechanotransduction and Extracellular Matrix Homeostasis," *Nat. Rev. Mol. Cell Biol.*, **15**(12), pp. 802–812.
- [7] Ambrosi, D., Ben Amar, M., Cyron, C. J., DeSimone, A., Goriely, A., Humphrey, J. D., and Kuhl, E., 2019, "Growth and Remodelling of Living Tissues: Perspectives, Challenges and Opportunities," *J. R. Soc. Interface*, **16**(157), p. 20190233.
- [8] Skalak, R., Dasgupta, G., Moss, M., Otten, E., Dullemeijer, P., and Vilmann, H., 1982, "Analytical Description of Growth," *J. Theor. Biol.*, **94**(3), pp. 555–577.
- [9] Rodriguez, E. K., Hoger, A., and McCulloch, A. D., 1994, "Stress-Dependent Finite Growth in Soft Elastic Tissues," *J. Biomech.*, **27**(4), pp. 455–467.
- [10] Fung, Y. C., Liu, S. Q., and Zhou, J. B., 1993, "Remodeling of the Constitutive Equation While a Blood Vessel Remodels Itself Under Stress," *ASME J. Biomech. Eng.*, **115**(4B), pp. 453–459.
- [11] Humphrey, J. D., and Rajagopal, K. R., 2002, "A Constrained Mixture Model for Growth and Remodeling of Soft Tissues," *Math. Models Methods Appl. Sci.*, **12**(03), pp. 407–430.
- [12] Klisch, S. M., Chen, S. S., Sah, R. L., and Hoger, A., 2003, "A Growth Mixture Theory for Cartilage With Application to Growth-Related Experiments on Cartilage Explants," *ASME J. Biomech. Eng.*, **125**(2), pp. 169–179.
- [13] Lanir, Y., 2015, "Mechanistic Micro-Structural Theory of Soft Tissues Growth and Remodeling: Tissues With Unidirectional Fibers," *Biomech. Model Mechanobiol.*, **14**(2), pp. 245–266.
- [14] Ateshian, G. A., 2007, "On the Theory of Reactive Mixtures for Modeling Biological Growth," *Biomech. Model Mechanobiol.*, **6**(6), pp. 423–445.
- [15] Giorgi, M., Carriero, A., Shefelbine, S. J., and Nowlan, N. C., 2014, "Mechanobiological Simulations of Prenatal Joint Morphogenesis," *J. Biomech.*, **47**(5), pp. 989–995.
- [16] Heegaard, J. H., Beaupre, G. S., and Carter, D. R., 1999, "Mechanically Modulated Cartilage Growth May Regulate Joint Surface Morphogenesis," *J. Orthop. Res.*, **17**(4), pp. 509–517.
- [17] Dixit, N. N., McFarland, D. C., and Saul, K. R., 2019, "Computational Analysis of Glenohumeral Joint Growth and Morphology Following a Brachial Plexus Birth Injury," *J. Biomech.*, **86**, pp. 48–54.
- [18] Shefelbine, S. J., and Carter, D. R., 2004, "Mechanobiological Predictions of Growth Front Morphology in Developmental Hip Dysplasia," *J. Orthop. Res.*, **22**(2), pp. 346–352.
- [19] Kainz, H., Killen, B. A., Wesseling, M., Perez-Boerema, F., Pitto, L., Garcia Aznar, J. M., Shefelbine, S., and Jonkers, I., 2020, "A Multi-Scale Modelling Framework Combining Musculoskeletal Rigid-Body Simulations With Adaptive Finite Element Analyses, to Evaluate the Impact of Femoral Geometry on Hip Joint Contact Forces and Femoral Bone Growth," *PLoS One*, **15**(7), p. e0235966.
- [20] Libby, J., Marghoub, A., Johnson, D., Khonsari, R. H., Fagan, M. J., and Moazen, M., 2017, "Modelling Human Skull Growth: A Validated Computational Model," *J. R. Soc. Interface*, **14**(130), p. 20170202.
- [21] Cobetto, N., Aubin, C. E., and Parent, S., 2020, "Anterior Vertebral Body Growth Modulation: Assessment of the 2-Year Predictive Capability of a Patient-Specific Finite-Element Planning Tool and of the Growth Modulation Biomechanics," *Spine (Phila Pa 1976)*, **45**(18), pp. E1203–E1209.
- [22] Zollner, A. M., Pok, J. M., McWalter, E. J., Gold, G. E., and Kuhl, E., 2015, "On High Heels and Short Muscles: A Multiscale Model for Sarcomere Loss in the Gastrocnemius Muscle," *J. Theor. Biol.*, **365**, pp. 301–310.
- [23] Budday, S., Steinmann, P., and Kuhl, E., 2015, "Secondary Instabilities Modulate Cortical Complexity in the Mammalian Brain," *Philos. Mag. (Abingdon)*, **95**(28–30), pp. 3244–3256.
- [24] Iranmanesh, F., and Nazari, M. A., 2017, "Finite Element Modeling of Avascular Tumor Growth Using a Stress-Driven Model," *ASME J. Biomech. Eng.*, **139**(8), p. 081009.
- [25] Cyron, C. J., Aydin, R. C., and Humphrey, J. D., 2016, "A Homogenized Constrained Mixture (and Mechanical Analog) Model for Growth and Remodeling of Soft Tissue," *Biomech. Model Mechanobiol.*, **15**(6), pp. 1389–1403.
- [26] Grytsan, A., Eriksson, T. S. E., Watton, P. N., and Gasser, T. C., 2017, "Growth Description for Vessel Wall Adaptation: A Thick-Walled Mixture Model of Abdominal Aortic Aneurysm Evolution," *Materials (Basel)*, **10**(9), p. 994.
- [27] Horvat, N., Virag, L., Holzapfel, G., Sorić, J., and Karšaj, I., 2019, "A Finite Element Implementation of a Growth and Remodeling Model for Soft Biological Tissues: Verification and Application to Abdominal Aortic Aneurysms," *Comput. Methods Appl. Mech. Eng.*, **352**, pp. 586–605.
- [28] Lin, W. J., Iafrafi, M. D., Peattie, R. A., and Dorfmann, L., 2018, "Growth and Remodeling With Application to Abdominal Aortic Aneurysms," *J. Eng. Math.*, **109**(1), pp. 113–137.
- [29] Mousavi, S. J., and Avril, S., 2017, "Patient-Specific Stress Analyses in the Ascending Thoracic Aorta Using a Finite-Element Implementation of the Constrained Mixture Theory," *Biomech. Model Mechanobiol.*, **16**(5), pp. 1765–1777.
- [30] Genet, M., Lee, L. C., Baillargeon, B., Guccione, J. M., and Kuhl, E., 2016, "Modeling Pathologies of Diastolic and Systolic Heart Failure," *Ann. Biomed. Eng.*, **44**(1), pp. 112–127.
- [31] Dixit, N. N., McFarland, D. C., Fisher, M. B., Cole, J. H., and Saul, K. R., 2020, "Integrated Iterative Musculoskeletal Modeling Predicts Bone Morphology Following Brachial Plexus Birth Injury (BPBI)," *J. Biomech.*, **103**, p. 109658.
- [32] Ateshian, G. A., Costa, K. D., Azeloglu, E. U., Morrison, B., 3rd., and Hung, C. T., 2009, "Continuum Modeling of Biological Tissue Growth by Cell Division, and Alteration of Intracellular Osmolytes and Extracellular Fixed Charge Density," *ASME J. Biomech. Eng.*, **131**(10), p. 101001.
- [33] Zhao, Y., Feng, B., Lee, J., Lu, N., and Pierce, D. M., 2020, "A Multi-Layered Model of Human Skin Elucidates Mechanisms of Wrinkling in the Forehead," *J. Mech. Behav. Biomed. Mater.*, **105**, p. 103694.
- [34] Cervera, F., 2002, "Thermal Expansion," *ASM Ready Reference: Thermal Properties of Metals*, ASM International, Materials Park, OH, pp. 9–10.
- [35] Maas, S. A., Ellis, B. J., Ateshian, G. A., and Weiss, J. A., 2012, "FEBio: Finite Elements for Biomechanics," *ASME J. Biomech. Eng.*, **134**(1), p. 011005.
- [36] Moerman, K. A., 2018, "GIBBON: The Geometry and Image-Based Bioengineering Add-On," *J. Open Source Software*, **3**(22), p. 506.
- [37] Ateshian, G. A., Morrison, B., 3rd, Holmes, J. W., and Hung, C. T., 2012, "Mechanics of Cell Growth," *Mech. Res. Commun.*, **42**, pp. 118–125.
- [38] Gray, D. J., Gardner, E., and O'Rahilly, R., 1957, "The Prenatal Development of the Skeleton and Joints of the Human Hand," *Am. J. Anat.*, **101**(2), pp. 169–223.
- [39] Tanck, E., Van Donkelaar, C. C., Jepsen, K. J., Goldstein, S. A., Weinans, H., Burger, E. H., and Huiskes, R., 2004, "The Mechanical Consequences of Mineralization in Embryonic Bone," *Bone*, **35**(1), pp. 186–190.